Ultra-low sintering temperature ceramic composites of $CuMoO_4$ through Ag_2O addition for microwave applications

Nina Joseph [a], Jobin Varghese [a], Merja Teirikangas [a], Mailadil Thomas Sebastian [a] and Heli Jantunen [a]

[a] Microelectronics Research Unit, Faculty of Information Technology and Electrical Engineering, P.O. BOX 4500, University of Oulu, FI-90014, Finland

Abstract

The present paper presents ceramic composites with ultralow sintering temperature of 500 °C with densification of 96 % by adding small amount (0.5, 1 and 2 wt.%) of Ag_2O to $CuMoO_4$ by simple mixing method. The effect of Ag_2O addition on the structure, microstructure, sintering and thermal as well as microwave dielectric properties of $CuMoO_4$ is also studied. The reduction in the sintering temperature is due to the formation of trace amount (1.4%) of copper silver molybdate ($Cu_2Ag_2(MoO_4)_3$) as observed from Rietveld refinement analysis as well as backscattered SEM image. Doping has very little influence on the structure and coefficient of thermal expansion that is about 4.7-5.2 ppm/°C. The composites sintered at 500 °C exhibit relative permittivity of about 8-9, quality factor (Qf) of 26000-37000 GHz at 12 GHz, temperature coefficient of resonant frequency of -31-33 ppm/°C and are compatible with Al electrode. The present work results in obtaining well-densified ultralow temperature cofired ceramic composites at low sintering temperature without much structural change and good thermal properties but with different dielectric properties by small doping. These composites can be used as low cost candidates for wide range of microwave applications like multilayer packages and substrates owing to the low energy required during processing and hence can pave way to the advancement of electronic materials.

Keyword : A. Ceramic-matrix composites (CMCs), B. Electrical properties, E. Sintering, Ultra low temperature cofired ceramics

Introduction

New advancements in materials, integration, packaging and interconnection technologies demand the miniaturization of millimetre wave components for wireless communication. In this application area, materials with feasible component permittivity, low dielectric loss (high Qf value), near-zero temperature coefficient, low sintering temperature below the melting points of the electrode metals, and chemical compatibility are required. A major option was the Low-Temperature Cofired Ceramic (LTCC) technology, which has gained increased attention in the research community due to its potential to fabricate novel multilayer modules involving the integration of passive components [1-11]. In the past 20 years, a significant number of ceramics with good microwave dielectric properties have been developed for LTCC applications [3]. The today's demand for energy saving, nontoxicity, and low cost limits the number of materials available for many practical applications.

In recent ten years or so, Ultra-Low Temperature Co-fired Ceramic (ULTCC) technology has been the focus of research as it can satisfy the urge of energy saving and reducing material wastage required by modern communication industry. In this technology, the targeted processing temperatures are below 700 °C, which enables the use of aluminium and nanosilver pastes as the inner electrodes. ULTCC materials with excellent dielectric properties and low sintering temperature have fascinated much attention due to its potential for numerous packaging and functional applications [12-14]. There are several ways to formulate microwave dielectric ceramics with ultra-low sintering temperature. The approaches used for LTCCs like utilization of low melting glass, low melting oxides, or small amounts of glass and metal oxides as sintering aids can be employed [12, 15,16].

Compositions like $K_2Mo_3O_{10}$ [17], $2Na_2O$-MoO_3 composite [18], $Li_3FeMo_3O_{12}$ [19], $Li_8Bi_2Mo_7O_{28}$ [20], $Te_2Mo_{0.95}W_{0.5}O_7$ [21], Pb_2WO_5 [22], $Li_3BiMo_3O_{12}$ [20], $Li_{0.5}Ce_{0.5}MoO_4$ [23], $(RbBi)_{0.5}MoO_4$ [24], $BaTe_4O_4$+40 wt.% $TiTe_3O_8$ [25], $(AgBi)_{0.5}(MoW)_{0.5}O_4$ [26], $(AgBi)_{0.5}WO_4$ [27], and $(LiBi)_{0.5}MoO_4$ [20] have the sintering temperature in the range of 500-600 °C, the relative permittivity (ε_r) of 5.6-45, the quality factor (Qf) of 300-36 000 GHz and the temperature coefficient of resonant frequency (τ_f) of -115 to 228 ppm/°C have been reported. However, the ULTCC ceramics with good microwave

properties are limited in number so far and from the practical applications point of view, further research is needed. Compositions with different relative permittivity but about the same sintering temperature are in great demand for multilayer applications. A simple and useful approach to obtain material with desired properties is by composite approach, which is widely utilized for many applications [28-42].

In our recent research, it was found that $CuMoO_4$ ceramic attained high density (96 %) with a moderately low sintering temperature of 650 ^oC. It exhibits excellent microwave and thermal properties with the relative permittivity (ε_r) of 8, quality factor (Qf) of 53 000 GHz, temperature coefficient of relative permittivity (τ_ε) = 63 ppm/^{o}C and temperature coefficient of resonant frequency (τ_f) = -36 ppm/^{o}C at 12.7 GHz. Moreover, $CuMoO_4$ showed low coefficient of thermal expansion of 4.6 ppm/^{o}C, which is close to semiconductor silicon (4 ppm/^{o}C) forming an additional advantage in the case of device level integration [43]. In addition to this, $CuMoO_4$ is also reported as a thermochromic and piezochromic ceramic as it displays a distinct reversible change in colour at around 200 K at ambient pressure and room temperature for a pressure of 250 MPa due to the structural rearrangement leading two distinct allotropic forms of α and γ [44-50]. Such chromic materials can find applications as user-friendly temperature and pressure indicators especially in safety improvement, medical, shock detector and packaging, etc. However even lower sintering temperature would be beneficial for decreasing the fabrication cost, saving energy and enabling seamless integration with temperature sensitive components and substrates. Hence, the present research focus on an attempt to lower its sintering temperature by using Ag_2O. Ag_2O was chosen due to its low melting point and has been successfully used earlier as a sintering aid in reducing the sintering temperature for ceramics like $SrBi_2Nb_2O_9$ and $Pb(ZrTi)O_3$ [51-53]. Ag_2O owing to its low decomposition temperature can results in obtaining a low melting compound on reaction of Ag with $CuMoO_4$. Hence can reduce the sintering temperature of $CuMoO_4$ as compounds having silver molybdates are reported to exhibit low sintering temperature with good dielectric properties [26, 54,

55]. By combining these two ingredients, we anticipate in obtaining a composite of ultra-low sintering temperature with feasible dielectric and thermal properties. The effect of Ag_2O addition on densification of $CuMoO_4$ is studied along with related structural and dielectric properties investigations. Furthermore, the compatibility of Al as an electrode material for Ag_2O modified $CuMoO_4$ is studied which is more specifically suitable for cost effective microwave applications.

Experimental

$CuMoO_4$ (CMO) ceramics was prepared by a solid-state oxide-mixing route from high purity oxides of CuO and MoO_3 (> 99 %, Alfa Aesar). The starting materials were weighed in stoichiometric amounts and ball milled in an absolute ethanol medium with yttria-stabilized zirconia (YSZ) balls for 24 hrs. The mixture was dried and calcined at 550°C for 12 hrs followed by further ball milling for 16 hrs to obtain powders with uniform particle size. Ag_2O (99+%, Alfa Aesar) with the amounts of 0.5, 1 and 2 wt.% were weighed and mixed with CMO in ethanol medium. Cylindrical disks were pressed (diameter 10 mm and thickness 5 mm) with 25 MPa and sintered in the temperature range of 350 - 550 °C for microwave measurements and microstructural studies.

The crystal structure of the powders was examined by X-ray diffractometer (D8, Bruker, Billerica, MA) using Cu Kα radiation while the slow scan X-ray diffraction of the powder was examined by X-ray diffractometer (Rigaku Smart Lab 9 kW, Germany) with scan rate of 0.01 using Co Kα radiation. The microstructure of the samples were characterized by scanning electron microscopy (FESEM, ZEISS Ultra Plus, Germany) and the bulk densities of the sintered samples by Archimedes method. The coefficient of thermal expansion (CTE) in the temperature range of 25-300°C was performed with dilatometer (NETZSCH, DIL 402 PC/4, Germany) using cylindrical samples (diameter 8 mm and length 15 mm) at a heating rate of 5 ^oC/min. The relative permittivity (ε_r) and quality factor were measured using Hakki Coleman and cavity method connected to a vector network analyser (10 MHz-20 GHz, ROHDE& SCHWARZ, ZVB20, Germany). The temperature coefficient of the resonant frequency (τ_f) in the temperature range of 25-85 ^oC was examined using cavity method with a

temperature chamber (SU-261, ESPEC CORP., Japan) and calculated using the equation 1, while temperature coefficient of relative permittivity (τ_ε) is calculated using equation 2 as shown below

$$\tau_f = \frac{f_{85} - f_{25}}{f_{25} * (85-25)} 10^{-6} \quad \text{ppm/}^{o}\text{C} \qquad (1)\ [56, 57]$$

$$\tau_\varepsilon = -2(\tau_f + \alpha_L)\ \text{ppm/}^{o}\text{C} \qquad (2)\ [58]$$

where α_L is the linear thermal expansion coefficient of the dielectric sample, τ_ε is the temperature dependence of the relative permittivity, and the τ_f is the resonance frequency of the sample at different temperatures.

Bosman and Havinga's correction [59] for the relative permittivity was calculated using the equation 3 for the porosity corrected relative permittivity, where *P* is the porosity of the dielectric sample

$$\varepsilon_{corrected} = \varepsilon_{measured}\,(1 + 1.5P) \qquad (3)$$

Results and discussion

Figure 1 depicts the X-ray powder diffraction pattern (XRPD) of pure and Ag_2O (0.5, 1 and 2 wt.%) added CMO sintered at 500 ^{o}C. All the peaks of pure CMO in the XRPD pattern is indexed based on CMO reported in the standard ICDD file card no: 073-0488 and 04-009-2226. It is also evident that the peak positions in the XRPD pattern of pure and doped CMO closely coincide, which indicate that this small doping of Ag_2O does not cause any noticeable alterations in the main crystal structure. In order to confirm the structure, a slow scan XRPD is carried out for 0.5 wt% of Ag_2O added CMO followed by Rietveld refinement using PDXL2 (Analysis incl. Rietveld). Figure 2 (a) shows the Rietveld refinement results of 0.5 wt.% Ag_2O added CMO sintered at 500 ^{o}C. The crystal structure of CMO is taken as starting model for Rietveld refinement as there is no observable changes in the structure by doping (figure 1) and all peaks are indexed by triclinic structure (P-1(2)) of CMO. The peaks are clearly visible in the XRPD pattern compared to the figure 1, due to the slow scan rate used for the characterization. The refinement was stable with low R-factors as shown in figure 2 (b). The refinement results reveal that the major phase of about 98.6 % (qualitative value) is $CuMoO_4$ and the

remaining 1.4 % (qualitative value) is that of secondary phase $Cu_2Ag_2(MoO_4)_3$ (ICDD File Card No: 01-078-2590). Table 1 shows the lattice parameters of major $CuMoO_4$ phase while that of the secondary phase is not given as it may not be precise owing to its weak XRPD peaks. The copper silver molybdate ($Cu_2Ag_2(MoO_4)_3$) (ICDD File Card No: 01-078-2590) has peaks at 2θ of 25.2, 25.5, 31.6 and 33.1°, which coincides with the peaks of CMO and are indexed in the figure 1. It is difficult to analyse the secondary phase due to the low concentration and hence further investigation is needed. The presence of secondary phase is also observed from backscattered electron image shown in figure 2 (c). The silver oxide may melt at around 300 °C and forms metallic silver which may react with the matrix to form the compound of copper silver molydate. During sintering at 500 ℃ and above, the new phase melted as observed from the SEM image, which further point out that it has low melting temperature of below 500 ℃ and hence may assist in the densification of the CMO. Similar observations were also reported [60-62].

Figure 3 shows the bulk density and densification of CMO composite ceramics as a function of the sintering temperature. The densification is calculated by comparing the bulk density of the composite to that of pure CMO ceramic, as it is difficult to obtain the theoretical density of the composite. The CMO composite ceramics exhibit an increase in density as the sintering temperature increases from 350 to 500 °C and remains almost constant at 500 °C. Moreover, the density also slightly increases with dopant concentration. This may be due to the presence of an additional phase as observed from figure 2. The densification also follows similar behaviour with increase in sintering temperature. Densification of 96 % is achieved for CMO ceramic by 0.5 wt.% addition of Ag_2O after sintering at 500 ^oC, being 150 ^oC lower than that for the pure CMO [43]. Further sintering at 550 ^oC results only in slightly improved densification. Similar results are obtained for 1 and 2 wt.% Ag_2O added samples and the achieved densifications are 96.3 % and 96.8 %, respectively at 500 ^oC. The reduction of sintering temperature may be due to the formation of trace amount of low melting compound, which enhances the densification rate at lower temperature [60-62]. Therefore, addition of Ag_2O can

promote faster grain growth that results in good densification at lower temperature. The conclusions according to the density measurements show that the preferred sintering temperature of the Ag_2O doped CMO ceramic is 500 ^oC.

The secondary electron images of the polished and thermally etched surface of the CMO composite ceramics after sintering at 450 ^oC, 500 ^oC and 550 ^oC are shown in figure 4. These images provide a good insight to the densification of CMO ceramic with Ag_2O addition in the sintering temperature range of 450-500 ^oC. The microstructure of the Ag_2O added CMO ceramics (0.5, 1 and 2 wt.%) sintered at 450 ^oC shown in figure 4 (a, b and c) exhibits some porosity which is in agreement with its densification values of 81, 85 and 87 % respectively. Further increase in sintering temperature to 500 ^oC (figure 4 d, e and f) results in much denser microstructure with almost uniform grains. SEM images of the sintered samples at 550 ^oC given in figure 4 (g, h and i) exhibit not much improvement in the densification. The microstructure of 0.5 wt.% of Ag_2O doped sample shows more uniform and homogeneous grains compared to the other doping levels. In general, the average grain size of the samples shows some increase in dopant concentration. It may be due to the rapid grain growth facilitated by the increase in Ag_2O content with results in more non-uniform grains owing to the formation of low melting new phase [63].

The measured CTE values (figure 5) of the CMO composite ceramics sintered at 500 ^oC in the temperature range of 25-300 ^oC are in the range of 4.7-5.2 ppm /^oC. This value being very close to the CTE value of Si, makes this composition interesting substrate for device level practical applications. The CTE slightly increases with increase in Ag_2O concentration and may be due to the contribution of the new phase formed.

The relative permittivity and Qf of CMO composite ceramics as a function of sintering temperature from 350 ^oC to 550 ^oC at about frequency of 12 GHz is presented in figure 6. As the sintering temperature is increased from 350 ^oC to 550 ^oC, both relative permittivity and Qf values also increased as expected. The rise is tremendous up to sintering temperature of 500 ^oC and further sintering to 550

^{o}C results only in a slight increase. These results are well in line with the density measurements and microstructure observed. It is also clear from the SEM images (figure 4) that there is an increase in the densification on increasing the temperature from 450 to 500 ^{o}C, and not much improvement at 550 ^{o}C. The relative permittivity increases from 3.8 to 8 with rise in sintering temperature from 350 ^{o}C to 500 ^{o}C and increases to 8.2 at 550 ^{o}C for 0.5 wt.% of Ag_2O added CMO. Similarly for 1 wt.% of Ag_2O added CMO, the relative permittivity changes from 3.8 to 8.3 for the same increase of temperature to 500 ^{o}C and became 8.5 at 550 ^{o}C. In the case of 2 wt.% of Ag_2O added CMO, the increase of relative permittivity is from 4.1 to 8.8 and then to 9.1 for the same sintering temperature increase. The porosity corrected value of relative permittivity for the 0.5, 1 and 2 wt.% of Ag_2O added samples sintered at 500 ^{o}C is 8.5, 8.8 and 9.2 respectively. The slight difference in the permittivity values of these composites can be accounted to their small difference in their densification (figure 3) as well as due to the presence of the new phase as evident from the SEM image (figure 2). Similar trend is followed in the variation of the Qf with temperature. For 0.5, 1 and 2 wt.% of Ag_2O added CMO, the Qf increases from 37000 to 39000 GHz, 32000 to 34000 GHz and 27000 to 28000 GHz, respectively, when the sintering temperature is increased from 500 ^{o}C to 550 ^{o}C. The small increase in both relative permittivity and Qf with an increase in sintering temperature above 500 ^{o}C may be due to the slight change in densification, which is clearly evident figure 3 and microstructure images (figure 4). Furthermore, the relative permittivity slightly increases while Qf decreases with increase in Ag_2O concentration in the CMO. It may corresponds to the Ag_2O addition due to the presence of small amount of new phase (copper silver molybdate) as evident from figure 2. The quality factor depends on many factors such a densification, pores, grain sizes/boundaries, and secondary phases etc. The grains appeared to be more uniform and homogeneous for 0.5 wt.% of Ag_2O doped sample, while growth is observed to be non-uniform with increase in dopant concentration as clear from the figure 4. The non-uniform grains due to the rapid grain growth with increase in dopant concentration may also account for the decrease in Qf value [63]. Further investigation is needed to know about the

dielectric properties of the new phase, as it is not well studied. Dielectric and structural properties of $Li_2(M^{2+})_2Mo_3O_{12}$ (M= An, Ca,In) ceramics with lyonsite related structures having ultra-low sintering temperature are reported while dielectric properties of copper silver molybdate is not reported [64]. The silver molybdate is reported to have ε_r of 8.1 and Qf of 17,000 GHz [65]. All the above observations indicate that the CMO-$Cu_2Ag_2(MoO_4)_3$ composite ceramics can be well sintered at 500 ^oC with good densification and microwave dielectric properties.

The temperature dependence of microwave dielectric properties of the ceramics is critical for practical applications. The resonant frequency of the CMO composite ceramics sintered at 500°C measured in the temperature range of 25°C to 85°C is shown in figure 7. As the temperature is increased from 25 ^oC to 85 ^oC, the resonant frequency slightly decreased linearly for 0.5, 1 and 2 wt.% of Ag_2O added CMO. Hence, the CMO-$Cu_2Ag_2(MoO_4)_3$ composite ceramics exhibit τ_f in the range of -31 to -33 ppm/^oC. The τ_ε is calculated from τ_f and CTE values using equation 2 and is found to be in the range of 52-56 ppm/^oC. The compatibility of Al as a material for electrodes with the CMO composite ceramics can be analysed by the XRPD and backscattered electron images of the cofired samples shown in figure 8. The XRPD (figure 8 a) shows peaks only related to CMO and Al which indicate that no interaction occurs between the ceramic and Al. The peaks of Al have higher intensity and may be due to the presence of 50 wt.% of Al metal, which is having large particle size that of matrix. SEM images of the cofired samples (figure 8 (b)) exhibit only two different type of grains where the darker grains belong to Al metal while the lighter one to matrix. Hence, Al metal can be used as an electrode for the CMO-$Cu_2Ag_2(MoO_4)_3$ composite ceramics. The larger grain size of the Al observed is due to the larger particle size of the Al initially used.

To understand the effect of Ag_2O on the properties of CMO, the properties of CMO composite ceramics sintered at 500 ^oC is compared to that of pure CMO (Table 2). It is evident that relative permittivity, τ_f and CTE of the CMO were not affected much by the Ag_2O addition while Qf decreases

with increase in Ag_2O addition. These composites can be accounted from the application point of view, considering the lowering of sintering temperature achieved along with good dielectric and thermal properties. Table 3 compares the microwave dielectric properties of some low sintering temperature materials (400-500 ^oC) with relative permittivity around 8 [17, 54, 55, 65]. The results indicate that Ag_2O doped CMO can serve as a potential candidate for ULTCC applications owing to its low sintering temperature with good densification while keeping the good dielectric and thermal properties.

Conclusions

Ultra-low temperature cofired ceramic composites with sintering temperature of 500 ^oC, and good densification of 96 % was achieved by adding $CuMoO_4$ with a small amount of Ag_2O by simple mixing method. The effect of addition on the microstructure, sintering, densification, thermal and microwave dielectric properties was investigated. The reduction in the sintering temperature is due to the formation of trace amount of copper silver molybdate ($Cu_2Ag_2(MoO_4)_3$) of about 1.4% as observed from Rietveld refinement analysis as well as backscattered SEM image. It was observed, that the Ag_2O doping has very little effect on the structure and the thermal expansion, which was 5 ppm/ ^oC. The doping has influence on the microwave dielectric properties especially the quality factor. The Ag_2O added (0.5, 1 and 2 wt.%) samples exhibit ε_r, Qf and τ_f in the range of 8-9, 37000-26000 GHz at about 12 GHz and -31 to -33 ppm/ ^oC, respectively. The CMO-$Cu_2Ag_2(MoO_4)_3$ composite ceramics are found to be compatible with Al electrode. The present work results in obtaining composites with different dielectric properties and good thermal properties at very low sintering temperature without much affecting the structure by small doping, which are useful for multilayer packages and substrates and can be applicable for other high temperature ceramics with good properties. Hence, $CuMoO_4$-$Cu_2Ag_2(MoO_4)_3$ composite ceramics with good densification, thermal and dielectric properties can be used as a promising material for various practical ULTCC applications.

Acknowledgement

The authors are thankful to European Research Council Project No: 24001893 for financial support.

References

1. Gupta TK, Jean JH. Principles of the Development of a Silica Dielectric for Microelectronics. J Mater Res 1996; 11: 243-263.
2. Bailey A, Foley W, Hageman M, Murray C, Piloto A, Sparks K, Zaki K. Miniature LTCC Filters for Digital Receivers. IEEE MMT-S Dig 1997; 2: 999-1002.
3. Sebastian MT, Jantunen H. Low Loss Dielectric Materials for LTCC Applications: A Review. Int Mater Rev 2008; 53: 57-90.
4. Axelsson K, Alford NM. Bismuth Titanates Candidates for High Permittivity LTCC. J Eur Ceram Soc 2006; 26: 1933-1936.
5. Valant M, Suvorov D. Chemical Compatibility between Silver Electrodes and Low-Firing Binary-Oxide Compounds: Conceptual Study. J Am Ceram Soc 2000; 83: 2721-2729.
6. Varghese J, Vahera T, Ohsato H, Jantunen H. Novel Low-Temperature Sintering Ceramic Substrate based on Indialite/Cordierite Glass-Ceramics. Jap J Appl Phys 2017; 56: 10PE01.
7. Surjith A, Ratheesh R. High Q ceramics in the $ACe_2(MoO_4)_4$ (A=Ba, Sr and Ca) system for LTCC applications. J Alloy Compd 2013; 550: 169-172.
8. Varghese J, Siponkoski T, Nelo M, Sebastian MT, Jantunen H. Microwave dielectric properties of low-temperature sinterable α-MoO_3. J Eur Ceram Soc 2017; In press: https://doi.org/10.1016/j.jeurceramsoc.2017.11.027.
9. Zhu X, Wang Z, Su X, Vilarinho PM. New Cu_3TeO_6 ceramics: phase formation and dielectric properties. ACS Appl Mater Interfaces 2014; 6: 11326-11332.
10. Zhou D, Guo D, Li, WB, Pang LX, Yao X, Wang D-W, Reaney IM. Novel temperature stable high-ε_r microwave dielectrics in the Bi_2O_3-TiO_2-V_2O_5 system. J Mater Chem C 2016; 4: 5357-5362.

11. Pang L-X, Zhou D, Qi Z-M, Liu W-G, Yue ZX. Reaney IM. Structure property relationships of low sintering temperature scheelite-structured (1-x)$BiVO_4$– x$LaNbO_4$ microwave dielectric ceramics. J Mater Chem C 2017; 5: 2695-2701.
12. Sebastian MT, Wang H, Jantunen H. Low temperature co-fired ceramics with ultralow sintering temperature: A review. Curr Opin Solid State Mater Sci 2016; 20: 151-170.
13. Subodh G, Sebastian M T. Glass free $Zn_2Te_3O_8$ microwave ceramic for LTCC applications. J Am Ceram Soc 2007; 90: 2266-2268.
14. Honkamo J, Jantunen H, Subodh G, Sebastian MT, Mohanan P. Tape casting and dielectric properties of $Zn_2Te_3O_8$ based ceramics with an ultra-low sintering temperature. Int J Appl Ceram Technol 2009; 6: 531-536.
15. Varghese J, Gopinath S, Sebastian MT. Effect of glass fillers in $Cu_2ZnNb_2O_8$ ceramics for advanced microwave applications. Mater Chem Phys 2013; 137: 811-815.
16. Varghese J, Siponkoski T, Teirikangas M, Sebastian MT, Uusimaki A, Jantunen H. Structural, dielectric, and thermal Properties of Pb free molybdate based ultralow temperature glass. ACS Sustainable Chem Eng 2016; 4: 3897-3904.
17. Zhang GQ, Guo J, He L, Zhou D, Wang H, Koruza J, Kosec M. Preparation and microwave dielectric properties of ultralow temperature sintering ceramics in K_2O-MoO_3 binary system. J Am Ceram Soc 2014; 97: 241-245.
18. Zhang G., Wang H, Guo J, He L, Wei DD, Yuan QB. Ultra low sintering temperature microwave dielectric ceramics based on Na_2O-MoO_3 binary system. J Am Ceram Soc 2015; 98: 528-533.
19. Liao Q, Wang Y, Jiang F, Guo D. Ultra low glass free $Li_3FeMo_3O_{12}$ microwave dielectrics. J Am Ceram Soc 2014; 97: 2394-2396.

20. Zhou D, Randall CA, Wang H, Pang LX, Yao X, Microwave dielectric ceramics in Li_2O-Bi_2O_3-MoO_3 system with ultra-low sintering temperatures. J Am Ceram Soc 2010; 93: 1096-1100.
21. Wang SF, Wang YR, Hsu YF, Lu HC, Tsai JS. Ultra-low fire $Te_2(Mo_{1-x}W_x)O_7$ ceramics: microstructure and microwave dielectric properties. J Am Ceram Soc 2010; 93: 4071-4074.
22. Xie HD, Xi HH, Chen C, Zhou D. Microwave dielectric properties of two low temperature sintering ceramics in the PbO–WO_3 binary system. Ceram Int 2015; 41: 10287-11092.
23. Pang LX, Zhou D, Guo J, Yue ZX, Yao X. Microwave dielectric properties of $(Li_{0.5}Ln_{0.5})MoO_4$ (Ln = Nd, Er, Gd, Y, Yb, Sm, and Ce) ceramics. J Am Ceram Soc 2015; 98: 130-135.
24. Zhou D, Randall CA, Pang LX, Wang H, Guo J, Zhang GQ, Wu Y, Guo KT, Shui L, Yao X. Microwave dielectric properties of $(AB)_{1/2}MoO_4$ (A = Li, Na, K, Rb, Ag) type ceramics with ultra-low firing temperatures. Mater Chem Phys 2011; 129: 688-692.
25. Wang SF, Wang YR, Hsu YF, Tsai JS. Densification, microstructure and microwave dielectric properties of ultra-low fire $BaTe_4O_9$-$TiTe_3O_8$ ceramic composites. J Eur Ceram Soc 2010; 30: 1737-1741.
26. Zhou D, Li WB, Guo J, Pang LX, Qi ZM, Shao T, Xie H-D, Yue ZX, Yao X. Structure phase evolution and microwave dielectric properties of $(Ag_{0.5}Bi_{0.5})$ $(Mo_{0.5}W_{0.5})O_4$ ceramic with ultra-low sintering temperature. Inorg Chem 2014; 53: 5712-5716.
27. Zhou D, Pang LX, Xie HD, Guo J, He B, Qi ZM, Shao T, Yao Xi, Randall CA. Crystal structure and microwave dielectric properties of an ultralow temperature fired $(AgBi)_{0.5}WO_4$ ceramic. Eur J Inorg Chem 2014; 2014: 296-301.
28. Xu S, Chen L, Gong M, Hu X, Zhang X, Zhou Z. Characterization and engineering application of a novel ceramic composite insulation material. Composites Part B 2017; 111: 143-147

29. Baryshnikov SV, Charnaya EV, Milinskii AYu, Antonov AA, Bugaev AS. Phase transitions in the $(BaTiO_3)x/(BiFeO_3)1-x$ composite ceramics: Dielectric studies. Composites Part B 2015; 80: 15-19.
30. Wang FJ, Li W, Xue MS, Yao JP, Lu JS. $BaTiO_3$-polyethersulfone nanocomposites with high dielectric constant and excellent thermal stability. Composites Part B 2011; 42: 87-91.
31. Halawani N, Auge JL, Morel H, Gain O, Pruvost S. Electrical, thermal and mechanical properties of poly-etherimideepoxy-diamine blend. Composites Part B 2017; 110: 530-541.
32. Su J, Zhang J. Improvement of mechanical and dielectrical properties of ethylene propylene diene monomer (EPDM)/barium titanate ($BaTiO_3$)by layered mica and graphite flakes. Composites Part B 2017; 112: 148-157
33. Brito-Pereira R, Ribeiro C, Lanceros-Mendez S, Martins P. Magnetoelectric response on Terfenol-D/ P(VDF-TrFE) two-phase composites. Composites Part B 2017; 120: 97-102.
34. Xu X-l, Yang C-j, Yang J-h, Huang T, Zhang N, Wang Y, Zhou Z-w. Excellent dielectric properties of poly(vinylidene fluoride) composites based on partially reduced graphene oxide. Composites Part B 2017; 109: 91-100.
35. Joseph N, Varghese J, Sebastian MT. Graphite reinforced polyvinylidene fluoride composites an efficient and sustainable solution for electromagnetic pollution. Composites Part B 2017; 123: 271-278
36. Suematsu K, Arimura M, Uchiyama N, Saita S, Makino T. Synthesis of $BaTiO_3$/polymer composite ink to improve the dielctric properties of thin films. Composites Part B 2016; 104: 80-86.
37. Hui D, Lau KT. The Revolutionary creation of new advanced materials- carbon nanotube composites. Composite Part B 2002; 33: 263-277.
38. Rajapakse YDS, Hui D. Marine Composites: Foreword. Composites Part B 2004; 35: 447-450.

39. Poh CL, Mariatti M, Noor AFM, Sidek O, Chuah TP, Chow SC. Dielectric properties of surface treated multi-walled carbon nanotube/epoxy thin film composites. Composites Part B 2016; 85: 50-58.
40. Goyal RK, Katkade SS, Mule DM. Dielectric, mechanical and thermal properties of polymer/$BaTiO_3$ composites for embedded capacitor. Composites: Part B 2013; 44:128-132.
41. Costa P, Silva J, Mendez SL. Strong increase of the dielectric response of carbon nanotube/ poly(vinylidene fluoride) composites induced by carbon nanotube and pretreatment, Composites Part B 2016; 93: 310-316.
42. Siponkoski T, Nelo M, Peräntie J, Juuti J, Jantunen H. $BaTiO_3$–P(VDF-TrFE) composite ink properties for printed decoupling capacitors. Composites: Part B 2015; 70: 201–205.
43. Joseph N, Varghese J, Siponkoski T, Teirikangas M, Sebastian MT, Jantunen H. Glass free $CuMoO_4$ ceramic with excellent dielectric properties for ultra-low temperature cofired ceramic applications. ACS Sustain Chem Eng 2016; 4: 5632-5639.
44. Ito T, Takagi H, Asano T. Drastic and sharp change in color, shape, and magnetism in transition of $CuMoO_4$ single crystals. Chem Mater 2009; 21: 3376-3379.
45. Thiry E, Gaudon M, Payen C, Daro N, Létard JF, Gorsse S, Deniard P, Rocquefelte X, Demourgues A, Whangbo MH, Jobic S. On the cyclability of the thermochromism in $CuMoO_4$ and its tungsten derivatives $CuMo_{1-x}W_xO_4$ ($x < 0.12$). Chem Mater 2008; 20: 2075-2077.
46. Yanasen I, Mizuno T, Kobayashi H. Structural phase transition and thermochromic behavior of synthesized W-substituted $CuMoO_4$. Ceram Int 2013; 39: 2059-2064.
47. Gaudon M, Riml C, Turpain A, Labrugere C, Delville MH. Investigation of the chromic phase transition of $CuMo_{0.9}W_{0.1}O_4$ induced by surface protonation. Chem Mater 2010; 22: 5905-5911.

48. Gaudon M, Deniard P, Demourgues A, Thiry AE, Carbonera C, Nestour AL, Largeteau A, Létard JF, Jobic S. Unprecedented "One-Finger-Push"-induced phase transition with a drastic color change in an inorganic material. Adv Mater 2007; 19: 3517-3519.
49. Shadduck H, Truckai C. Medical instrument with thermochromic or piezochromic surface indicators. US 20030216732 A1 (2003).
50. Gutierrez VB, Cornu L, Demourgues A, Gaudon M. $CoMoO_4/CuMo_{0.9}W_{0.1}O_4$ mixture as an efficient piezochromic sensor to detect temperature/pressure shock parameters. ACS Appl Mater Interfaces 2015; 7: 7112-7117, DOI: 10.1021/am508652h.
51. Hu Z-S, Hung F-Y, Chang S-J, Hsieh W-K, Chen K-J. Align Ag nanorods via oxidation reduction growth using RF-sputtering. J Nanomater 2012; 2012: Article ID 345086, 1-6, doi:10.1155/2012/345086.
52. Wang C, Fang QF, Zhu ZG. Enhanced dielectric properties of low temperature sintered $SrBi_2Nb_2O_9$/Ag composites. Appl Phys Lett 2002; 80: 3578-3580.
53. Hwang HJ, Watari, K, Sando M, Toriyama M. Low temperature sintering and high strength $Pb(Zr,Ti)O_3$- matrix composites incorporating silver particles. J Am Ceram Soc1997; 80: 791-793.
54. Zhou D, Pang L-X, Qi Z-M, Jin B-B, Yao X. Novel ultra- low temperature cofired microwave dielectric ceramic at 400 degrees and its chemical compatibility with base metal. Sci Rep 2014; 4: 5980 (1-4).
55. Zhou D, Li J, Pang L-X, Wang D-W, Reaney M.. Novel water insoluble $(Na_xAg_{2-x})MoO_4$ ($0 \leq x \leq 2$) microwave dielectric ceramics with spinel structure sintered at 410 degrees. J Mater Chem C 2017; 5: 6086-6091.
56. Sebastian MT. Dielectrics for wireless communications. Elsevier, 2008, UK.
57. Pang LX, Liu WG, Zhou D, Yue ZX. Novel glass free low temperature fired microwave dielectric ceramics: $Bi(Ga_{1/3}Mo_{2/3})O_4$. Ceram Int 2016; 42: 4574-4577.

58. Chiang C, Wang SF, Wang YR, Wei WCJ. Densification and microwave dielectric properties of CaO-B_2O_3-SiO_2 system glass-ceramics. Ceram Int 2008; 34: 599-604.
59. Bosman J, Havinga EE. Temperature dependence of dielectric constants of cubic ionic compounds. Phys Rev 1963; 129: 1593-1600.
60. Jeong B-J, Joung M-R, Kweon S-H, Kim J-S, Nahm S, Choi J-W,Hwang S-J. Effect of Bi_2O_3 doping on the sintering temperature and microwave dielectric properties of $LiAlSiO_4$ J Am Ceram Soc2012; 95: 1811-1813.
61. Zhang TS, Ma J, Kong LB, Chan SH, Hing P, Kilner JA. Iron oxide as an effective sintering aid and a grain boundary scavenger for ceria-based electrolytes. Solid State Ionics 2004; 167: 203-207.
62. Tianshu Z, Hing P, Huang H, Kilner J. Early-stage sintering mechanisms of Fe-doped CeO_2. J Mater Sci 2002; 37: 997-1003.
63. Lee Y, Yoo J, Lee K, Kim I, Song J, Park YW. Dielectric and piezoelectric characteristics of the non-stoichiometric (Na,K)NbO_3 ceramics doped with CuO. J Alloys Compd 2010; 506: 872-876.
64. Zhou D, Randall CA, Pang LX, Wang H, Wu XG, Guo J, Zhang G-Q, Shui L, Yao X. Microwave dielectric properties of $Li_2(M^{2+})_2Mo_3O_{12}$ and $Li_3(M^{3+})Mo_3O_{12}$ (M = Zn, Ca, Al, and In) lyonsite related type ceramics with ultra-low sintering temperatures. J Am Ceram Soc 2011; 94: 802–805.
65. Zhou D, Li W-B, Pang L-X, Guo J, Qi Z-M, Shao T, Yue Z-X, Yao X. Sintering behavior and dielectric properties of ultra-low temperature fired silver molybdate ceramics. J Am Ceram Soc 2014; 97: 3597-3601.

Tables

Table 1 Refined lattice parameters

Lattice parameters	$CuMoO_4$
a (Å)	6.7876 (0.00017)
b (Å)	8.3734 (0.00021)
c (Å)	9.9056 (0.00025)
Volume (Å^3)	518.8670 (0.0232)
Quantitative value (%)	98.6165 (0.4055)
Space group	P-1(2)

Table 2 Comparison of the properties of pure and Ag_2O doped CMO

Properties	**CMO**	**Ag_2O doped CMO (wt. %)**		
	[43]	**0.5**	**1**	**2**
S.T$^{\#}$(^{o}C)	650	500	500	500
Densification (%)	96	96.0	96.3	96.8
Qf (GHz)	53000	37000	32000	26000
ε_r	7.9	8.0	8.3	8.8
Porosity corrected ε_r #	8.4	8.5	8.8	9.2
τ_f (ppm/^{o}C)	-36	-32	-31	-33
CTE (ppm/^{o}C)	4.6	4.7	4.9	5.2

S.T.: Sintering Temperature

Table 3 Comparison of microwave dielectric properties of some low sintering temperature dielectric ceramics (400-500 ^{o}C)

Composition	**S.T$^{\&}$ (^{o}C)**	**ε_r**	**Qf (GHz)**	**τ_f (ppm/^{o}C)**	**Reactivity with Ag or Al**	**Ref.**
$NaAgMoO_4$	400	7.9	33000	-120	-	**54**
$(Na_{1.2}Ag_{0.8})MoO_4$	**410**	**8.1**	**44800**	**-82**	**-**	**55**
Ag_2MoO_4	450	8.1	17000	-133	-	**65**
$K_2Mo_2O_7$	460	7.5	22300	-63	Yes for Ag, no for Al	**17**
CMO-0.5 Ag_2O	500	8.0	37000	-32	Yes for Ag, no for Al	This work
CMO-1 Ag_2O	500	8.3	32000	-31	Yes for Ag, no for Al	This work
CMO-0.5 Ag_2O	500	8.8	26000	-33	Yes for Ag, no for Al	This work

& S.T.: Sintering Temperature

Figure captions

Figure 1 X-ray powder diffraction pattern of pure CMO and Ag_2O (0.5, 1, 2 wt%) **added** CMO sintered at 500 ^oC.

Figure 2 (a) Slow scan X-ray powder diffraction pattern and Rietveld refinement results, (b) refinement fitness and (c) back scattered electron image of 0.5 wt % Ag_2O **added** CMO sintered at 500 ^oC.

Figure 3 **(a) Bulk density and (b)** densification of CMO **composite ceramics** with sintering temperature in the range of 350 - 550 ^oC.

Figure 4 Microstructure (SE2 image) of CMO doped with Ag_2O (a) 0.5 (b) 1 (c) 2 wt.% sintered at 450 ^oC, (d) 0.5 (e) 1 (f) 2 wt.% sintered at 500 ^oC, (g) 0.5 (h) 1 (i) 2 wt.% sintered at 550 ^oC.

Figure 5 Thermal expansion of CMO **composite ceramics** sintered at 500 ^oC in the temperature range of 25 - 300 ^oC.

Figure 6 (a) ε_r and (b) Qf of CMO **composite ceramics** as a function of sintering temperature at 12 GHz.

Figure 7 Variation of resonant frequency of CMO **composite ceramics** sintered at 500 ^oC as a function of temperature.

Figure 8 (a) XRD (b) Back scattered electron images of 2 wt.% Ag_2O **added** CMO with 50 wt.% of Al cofired at 500 ^oC.

Figures

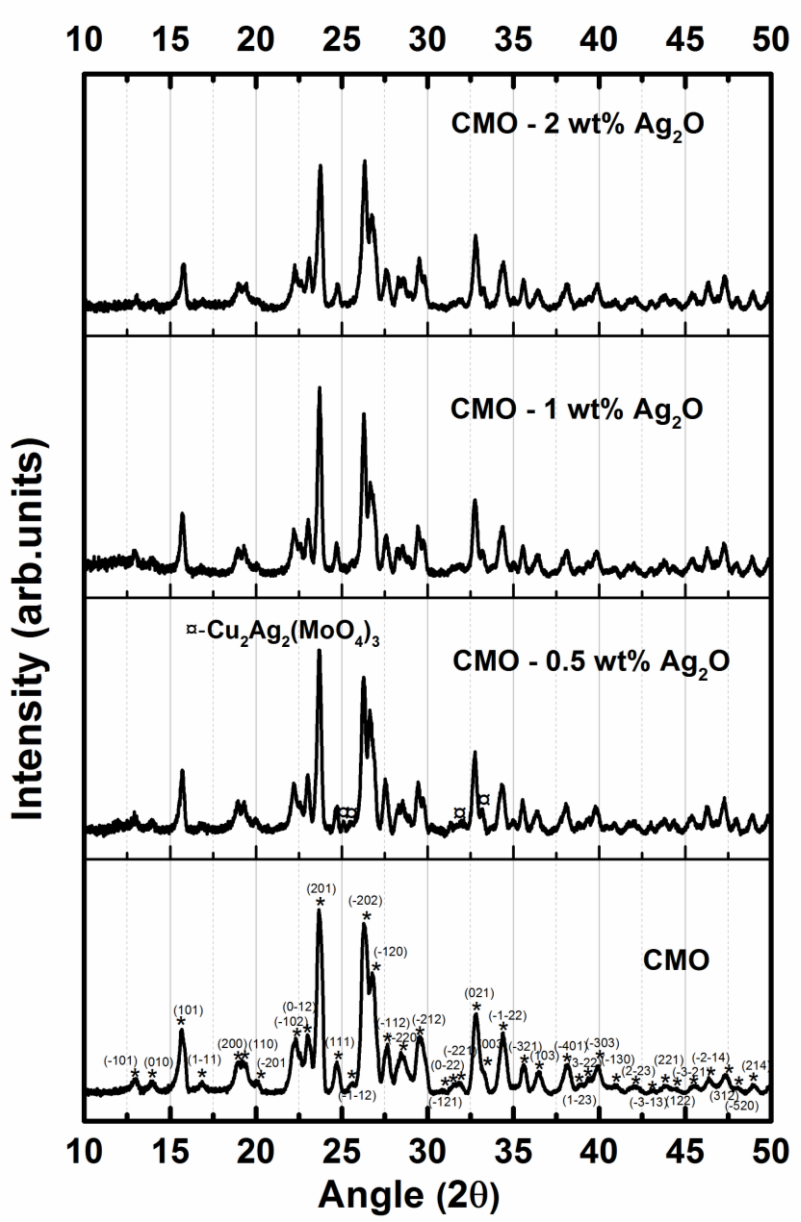

Figure 1

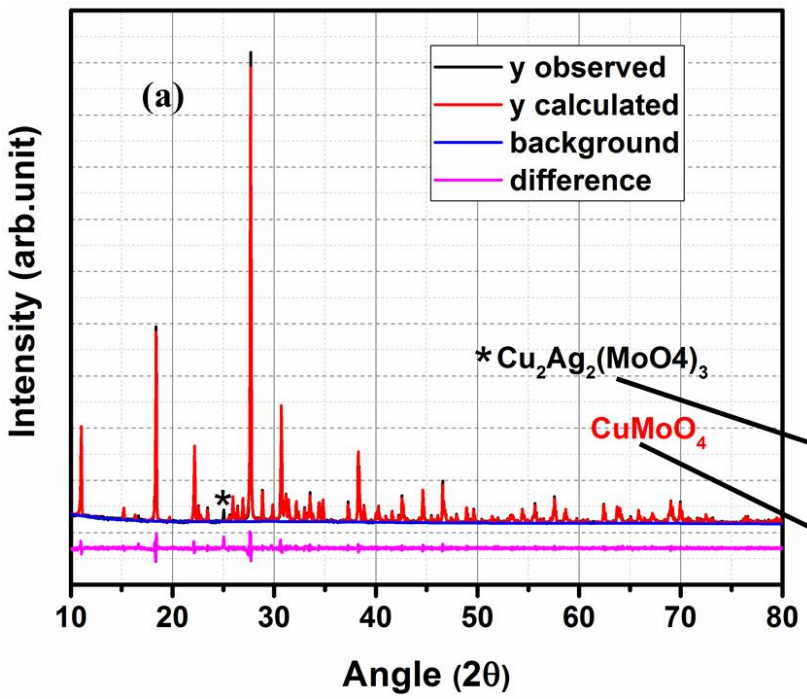

(b)

Refinement parameters	Values
R_{wp}	5.18 %
R_p	3.88 %
R_e	3.96 %
S	1.3073
χ^2	1.7089
Maximum shift/e.s.d.	1.627

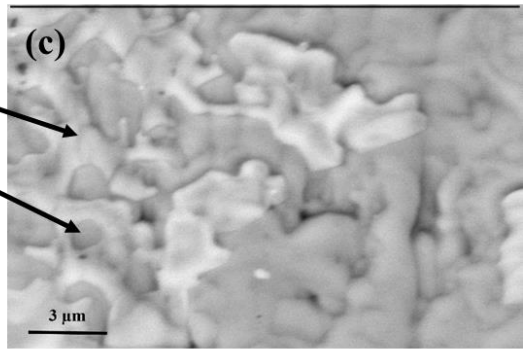

Figure 2

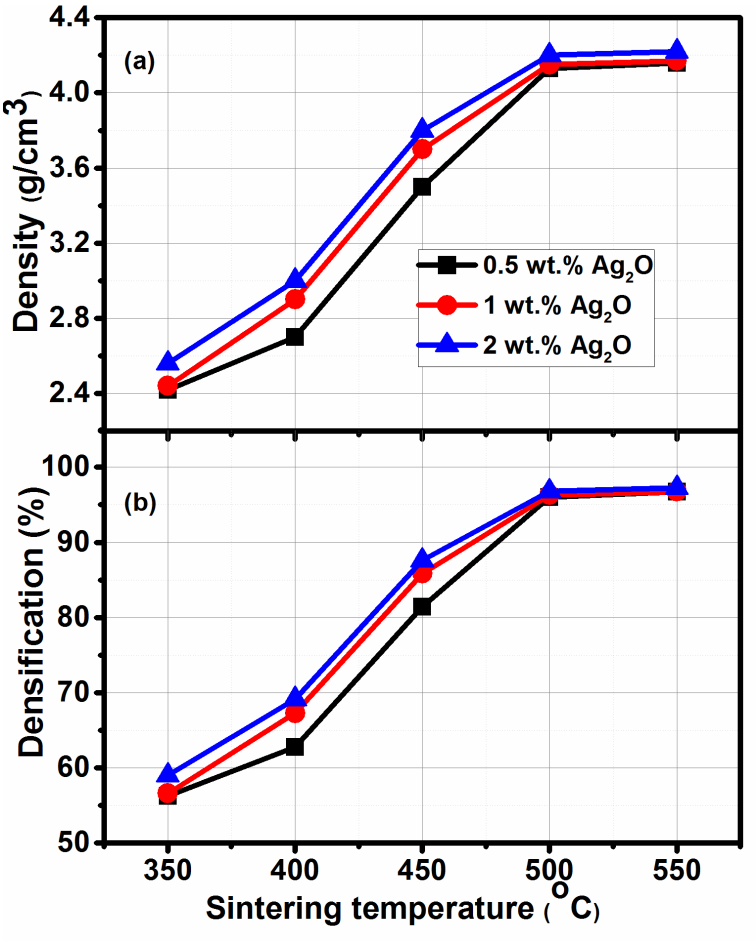
(a)
Density (g/cm3)
4.4
4.0
3.6
3.2
2.8
2.4
0.5 wt.% Ag2O
1 wt.% Ag2O
2 wt.% Ag2O
(b)
Densification (%)
100
90
80
70
60
50
350
400
450
500
550
Sintering temperature (oC)

Figure 3

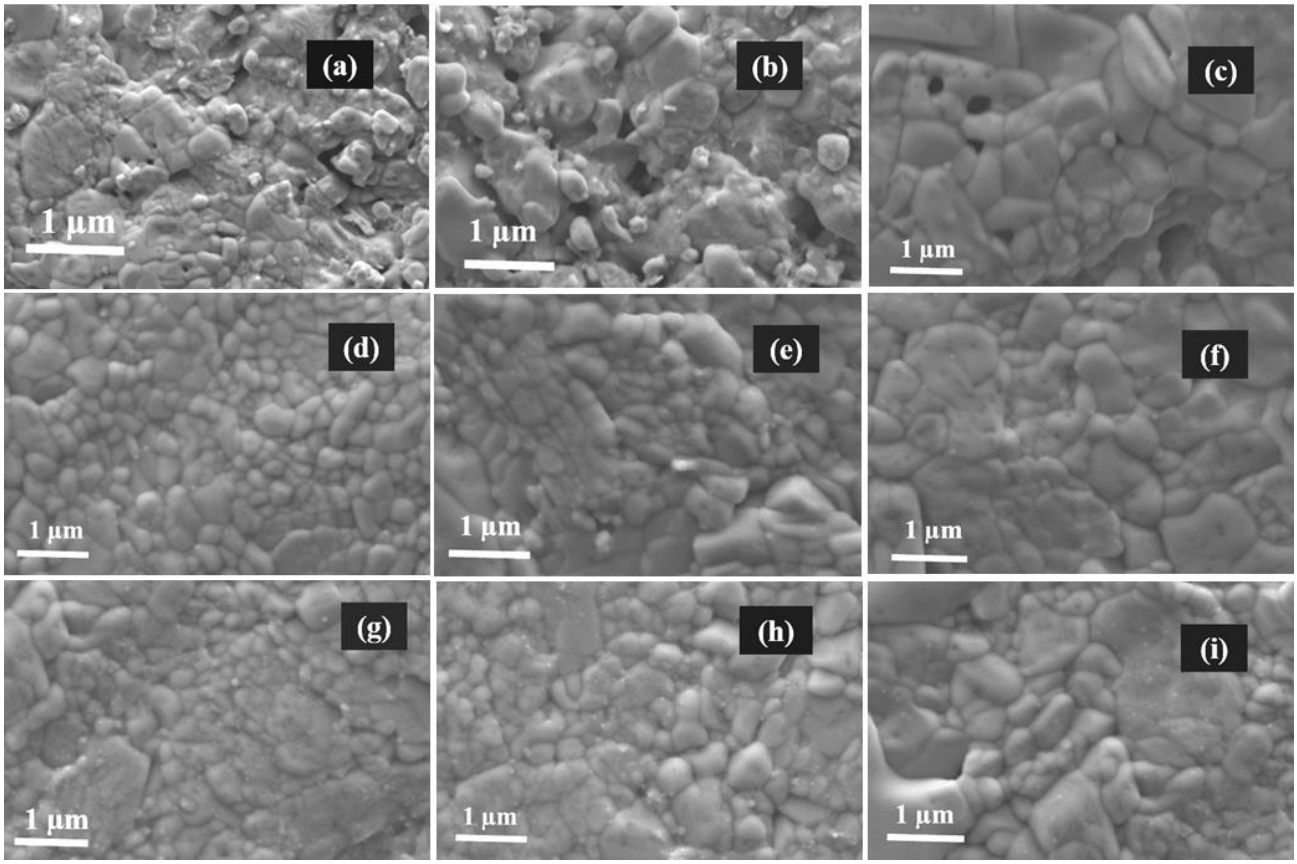

Figure 4

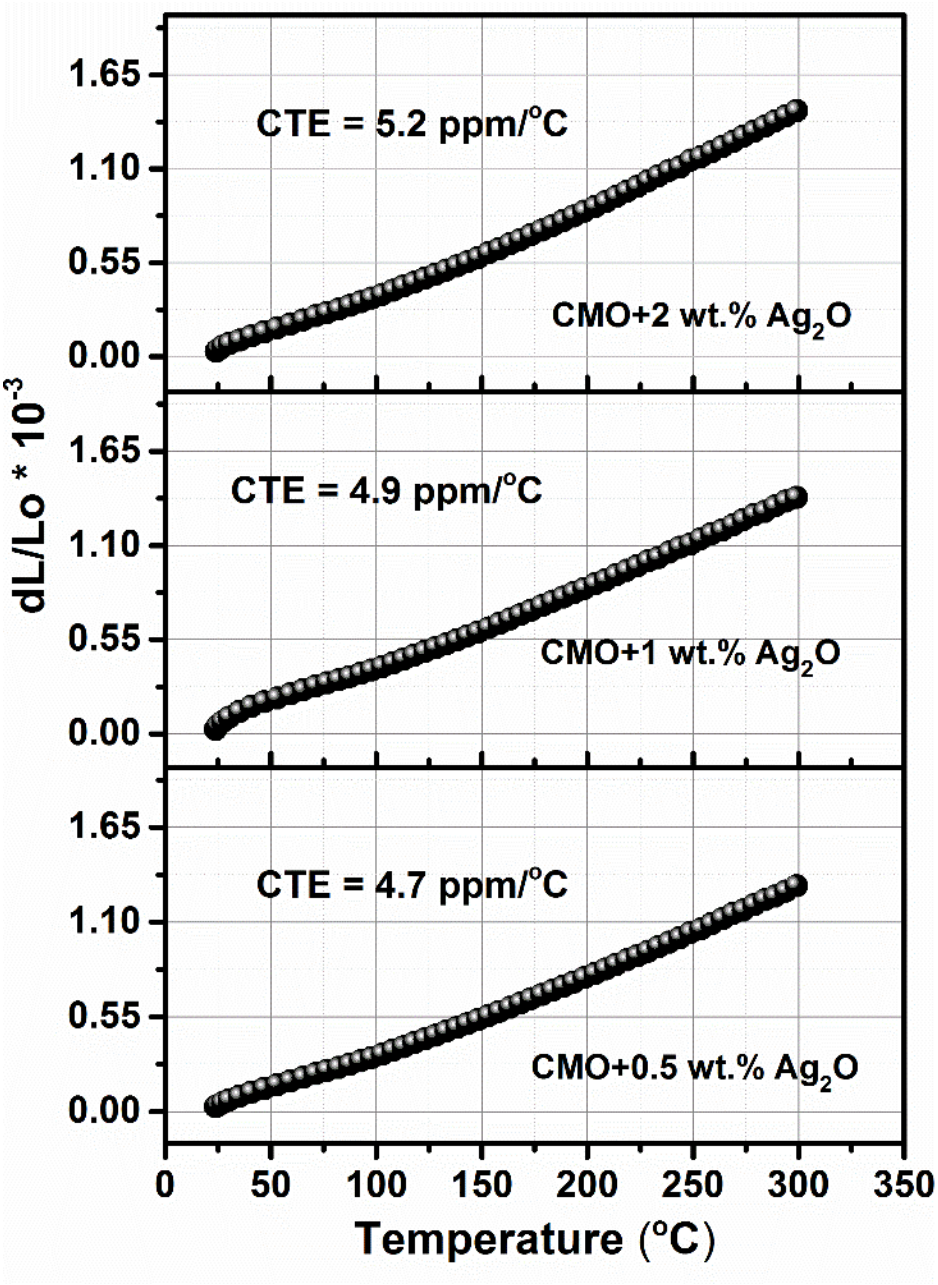
CTE = 5.2 ppm/°C
CMO+2 wt.% Ag2O
CTE = 4.9 ppm/°C
CMO+1 wt.% Ag2O
CTE = 4.7 ppm/°C
CMO+0.5 wt.% Ag2O
dL/Lo * 10-3
Temperature (°C)
1.65
1.10
0.55
0.00
0
50
100
150
200
250
300
350

Figure 5

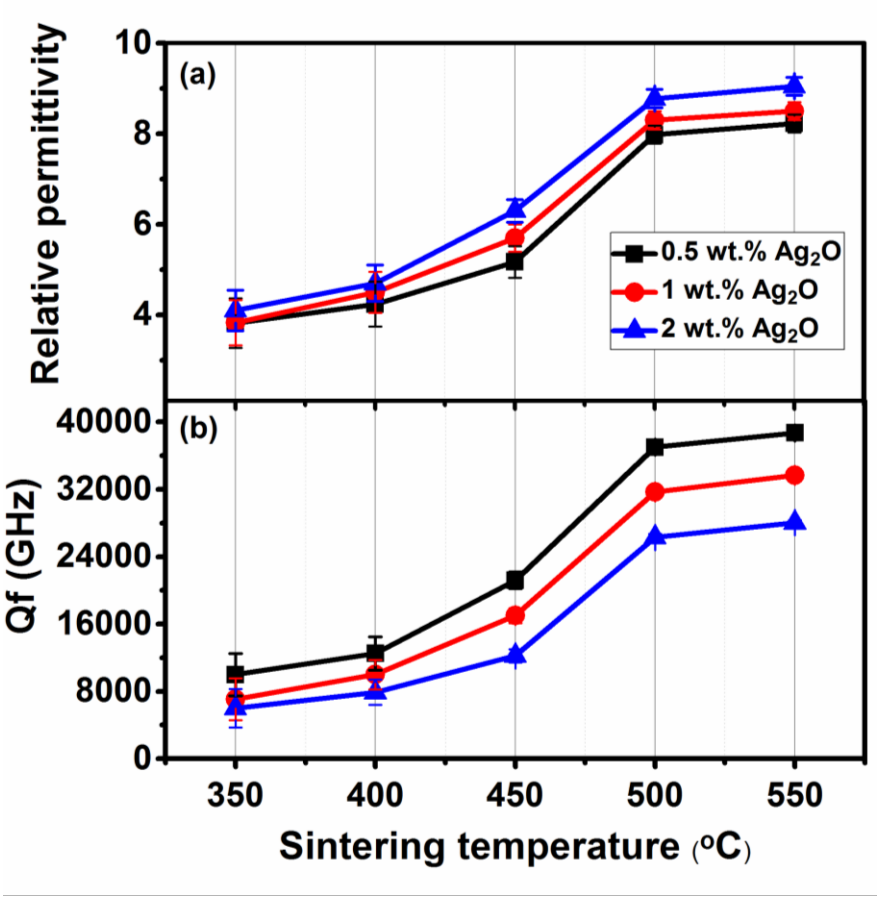
(a)
(b)
Relative permittivity
Qf (GHz)
Sintering temperature (°C)
0.5 wt.% Ag2O
1 wt.% Ag2O
2 wt.% Ag2O
10
8
6
4
40000
32000
24000
16000
8000
0
350
400
450
500
550

Figure 6

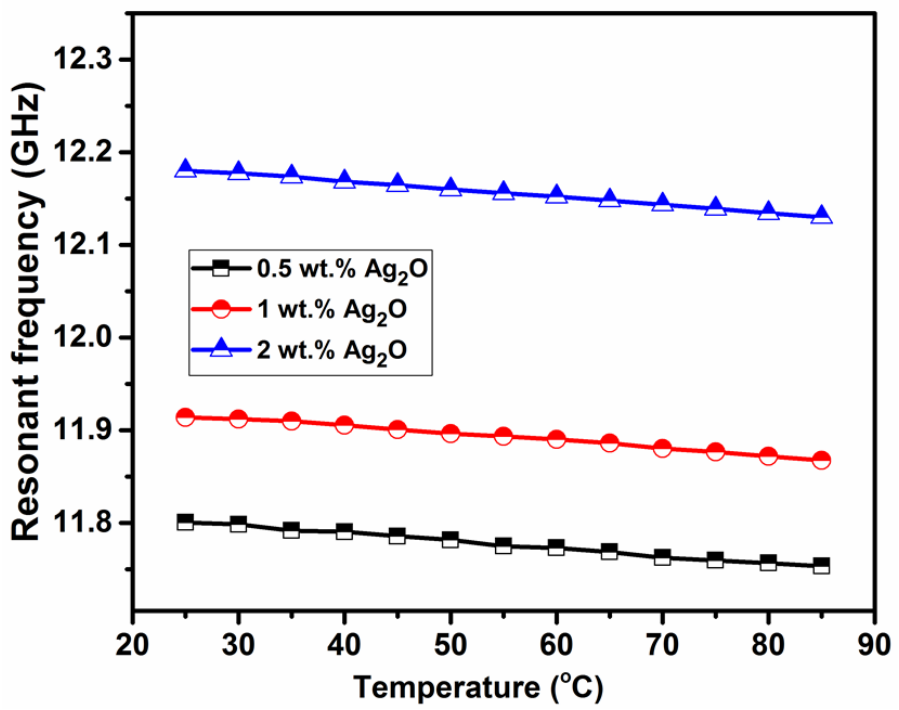

Figure 7

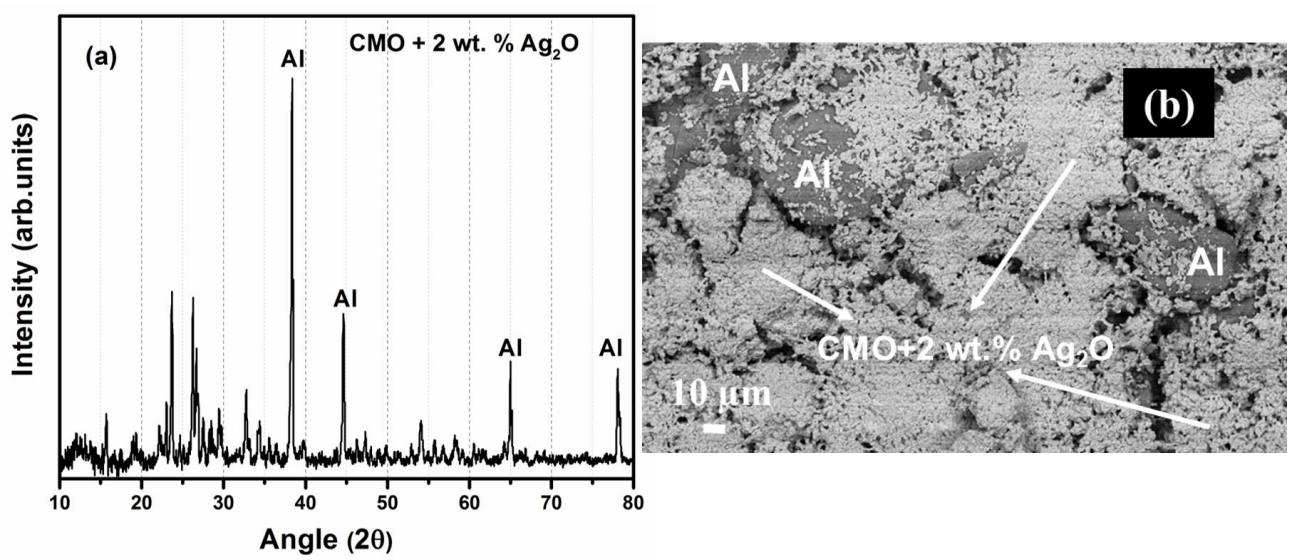

Figure 8